Kirk-Othmer Encyclopedia of Chemical Technology.

MEDICAL IMAGING TECHNOLOGY

Medical imaging is the application of nonsurgical techniques to produce images of internal organs and tissues. Imaging has become an indispensable tool to the medical community, providing information otherwise obtainable only by invasive exploratory procedures. Imaging technology can be used to determine if a persistent headache is caused by a brain tumor, or if a fetus is developing normally. This technology can sometimes go beyond locating pathology; in some cases it can identify the type of pathology. For example, it is often possible to distinguish between images of benign and malignant tumors, thus eliminating the need for some invasive procedures. Imaging technology has also extended the frontiers of medicine in many areas. Mapping brain functions and fetal surgery *in utero* are two examples (see also Nondestructive evaluations).

The five principal imaging technologies involve optical, x-ray, ultrasound, radio frequency (rf), or nuclear techniques. Additionally, medical imaging relies heavily on hundreds of ancillary chemical, computer, detector, electronic, film, and magnetic technologies developed in the latter twentieth century. The discussion herein includes basic imaging principles, and endoscopic, x-ray, ultrasound, magnetic resonance, and nuclear imaging as found in hospitals. Endoscopy is a general term used to describe any optical medical imaging technique producing images of the inside of the body by the insertion into the body of an optical imaging device, such as a small video camera, fiber optic viewer, or light pipe. X-ray imaging includes plane film and computerized tomography (CT) imaging techniques, both based on the absorption of x-rays passing through the body. X-ray imaging is used for hard tissues, such as bones, and soft tissues. Ultrasound imaging, based on the reflection of ultrasonic sound waves by the tissues of the body, is primarily used for soft tissue imaging. Magnetic resonance imaging (MRI) is based on the absorption of radio frequency waves by certain nuclei in the body when placed in a magnetic filed. MRI is used to image both soft and hard tissues of the human body, as well as to determine brain function. Nuclear imaging results from measuring γ-rays given off by radioactive compounds, ie, radiopharmaceuticals (qv), introduced into the body. Nuclear imaging is primarily used to image the functionality of an organ which has an affinity for an exogenous radioactive tracer.

1. Basic Imaging Principles

An image is a matrix of picture elements (pixels) representing the magnitude of the imaged quantity in a given location. Images may be produced by absorption, emission, or reflection of energy by body tissue. Absorption techniques gather information by passing electromagnetic radiation through the body. The spatial variation in intensity of the energy absorbed by the tissues is used to produce an image of the internal organs. Reflection techniques rely on variations in the reflected energy from a tissue or organ. Emission techniques are based on variations in the intensity of energy emitted by the body resulting from the excitation of tissues by an external stimulus, or the introduction of an emissive substance which collects in a specific tissue.

The signal in an image is defined as the intensity of the energy arising from the imaged tissue. The contrast between two tissues in an image is the difference between the signals of the two tissues. The signal-to-noise ratio (SNR) of a tissue in a medical image is the ratio of the signal intensity of that tissue to the noise

level in the image. The SNR is not the best indicator of image quality. Rather, the contrast-to-noise ratio (CNR) between adjacent tissues is the factor which determines the utility of an image, provided sufficient signal exists.

Medical images are annotated with the conventional medical nomenclature for the directions of left, right, superior (toward the head), inferior (toward the feet), anterior (toward the front), and posterior (toward the back) of the body. There are three standard planes: one which is perpendicular to the long axis of the body and divides the body into superior and anterior parts is referred to as an axial plane, one which divides the body into left and right halves is called a sagittal plane, and one dividing the anterior from the posterior is referred to as a coronal plane. An oblique plane is one which lies between the three standard planes. For example, an oblique axial–sagittal plane is one which lies between an axial and sagittal plane. Anatomy further away from a reference point is distal and that which is closer is proximal.

Information from an imaging session may be presented as a projection, tomographic, or volume image. Projection images represent the energy coming out of the imaged anatomy. This image is similar to the shadow obtained by placing a hand in front of a light bulb. A single projection image contains no information about the depth of the absorbing tissues. However, anterior-to-posterior and posterior-to-anterior projection images together contain some depth information owing to the point source nature of the source. Tomographic images are images of a thin slice of thickness (Thk) through the body. The thin slice is composed of small-volume elements (voxels), the signal content of which is represented as intensity in the corresponding pixel. Tomographic images are referred to as axial, sagittal, coronal, or oblique. Volume images are three-dimensional (3-D) representations of the organs and tissues. In general, tomographic and volume images require more elaborate imaging hardware than do projection images.

2. Endoscopy

Endoscopy, the use of optical instruments to image the inside of the human body, was perhaps the first medical imaging modality (1). In the early 1800s small, hollow, rigid tubes were used to examine the larynx and pharynx. These early instruments passed candle light down the tubes to illuminate the organs being viewed. In 1868 Kussmaul saw the inside of the stomach by having the subject, a sword swallower, swallow a 13-mm diameter 47-cm length rigid tube (2). The light source was dim, and the view quickly obscured by the digestive fluids in the stomach. By 1879 the Nitze-Leiter cystoscope was available, but extremely cumbersome for examination of the urinary bladder (1). Minor advances in the 1890s made the endoscope bendable through small angles and improved the light source. The principal breakthrough for endoscopy came in the 1950s with the development of fiber optics (qv). A flexible bundle of fiber optics placed in the body gave images of organs not imagable by rigid pipes. The fiber optics could also be used to provide a light source to view the imaged organ. Moreover, the introduction of flexible fiber optic endoscopes lowered the probability of puncturing an organ which sometimes occurred with rigid light pipes. The next breakthrough in optical imaging was the development in the 1980s of the charge-coupled device (CCD) video camera. A small CCD camera measuring a few millimeters in diameter inserted into the body produces clear images of the internal organs.

2.1. Theory and Equipment

Many diseases of the human body can be identified by visual appearance. Tumors in the upper gastrointestinal (GI) tract, for example, possess a characteristic salmon pink color (3). The presence of such a color can be an indication of disease. Endoscopy is the medical imaging tool used to detect such colors in the inside of hollow internal organs such as the rectum, urethra, urinary bladder, stomach, colon, etc. An endoscope is the instrument used to perform endoscopy. Endoscopic imaging involves the production of a true color picture of

the inside of the human body using lenses and either hollow pipes, a fiber optic bundle, or a small CCD camera. All three use a large field-of-view, sometimes referred to as a fish eye, lens to allow a 180° field of view.

The hollow pipe approach uses a small-diameter hollow pipe through which an image from a carefully designed optical system is transmitted. An image is viewed at the end of the pipe external to the body using the appropriate optical eyepiece or video camera. Some devices possess flexible elbows and internal mirrors which allow the pipe to be bent by small angles. Illumination of the object at the end of the pipe is accomplished by sending light down the pipe.

Alternatively, a fiber optic bundle can be used in place of the pipe. In a fiber optic bundle, a matrix of small (50–100 μm) fiber optic strands are arranged such that the ordering of the strands at one end is equivalent to that on the other end. Therefore an image focused on one end with lenses is transmitted to the other end. Light is typically sent down some of the fibers not used for image transmission to provide illumination.

Endoscopes containing a CCD camera replace the fiber optic bundle with a small monochrome CCD chip at the focal point of the fish eye lens (4). The chip contains approximately 512×512 picture elements (pixels). The tissues being imaged are illuminated with light from a few of the fiber optic strands. Color images are produced by alternately illuminating with red, green, and blue light. Data from the CCD chip is therefore a series of red, green, blue, red, green, blue, etc, images which are processed to produce the color video. Endoscopes of this form typically have a camera system connected to an external TV monitor, a fiber optic light source, a tube for rinsing the camera lens with water, and a small tube for insertion of a needle or forceps device for collecting biopsy samples. This combination of implements fits into a flexible 1-cm tube.

2.2. Applications

Endoscopy finds applications in a number of investigations of the inside of the human body. It is typically performed using a local anesthetic. Arthroscopy is the examination of a joint using an optical device called an arthroscope which is inserted into a joint through a hole in the skin (5). The arthroscope may be purely optical in construction or contain a miniature electronic camera external to the arthroscope. Cystoscopy is the use of an endoscope to examine the entire urinary tract from the urethra to renal calyx (6). Laparoscopic surgery is surgery using small slender surgical instruments inserted through incisions in the abdomen (7). The surgery is guided with a laparoscope, a slender rigid optical instrument having an external CCD camera inserted into the body. Several surgical techniques can be performed in the peritoneal cavity with only minor incisions for the laparoscope and operating tools: fetoscopy is the visualization of the fetus using a small-diameter needlescope (8); bronchoscopy is the examination of the bronchial tree in the lungs (9); and laryngoscopy is the examination of the larynx (10).

The largest use of endoscopic techniques is in the examination of the gastrointestinal tract. Upper intestinal endoscopy is the examination of the esophagus, stomach, and proximal duodenum. Colonoscopy is the examination of the colon, large intestine, and in some cases the distal parts of the small intestine. Cholangiopancreatography is the examination of the biliary tree and pancreas.

Each of the endoscopic imaging procedures is relatively risk free and painless when performed by competent and well-trained individuals using a local anesthetic. Fetoscopy has the highest risk. There is a 10% increased probability of premature delivery and 10% higher fetal loss rate.

3. X-Ray Imaging

X-ray medical imaging is the most mature and widely used of the diagnostic imaging modalities (see X-ray technology). X-ray imaging began with the discovery of x-rays in 1895 by Wilhelm Röntgen (11). Combining x-ray technology and fluorescent screen technology allowed views of the inside of objects. X-ray imaging had a great and rapid impact on society and Röntgen was awarded a Nobel Prize six years after his discovery.

4 MEDICAL IMAGING TECHNOLOGY

Applications of x-ray imaging to soft tissue came in the 1910s with the development of contrast agents. Compounds of barium were found to absorb x-rays more than the soft tissues of the GI tract, allowing the intestine of a patient who ingested barium to be imaged. The imaging of blood vessels was first demonstrated in 1896 by introducing an x-ray opaque solution into the blood vessels of a cadeveric hand (12). The less invasive form of blood vessel imaging known as angiography was developed in the late 1920s. In the 1970s, driven by safety concerns, higher efficiency intensifier screens and photographic films were developed reducing the required dose of x-ray radiation by as much as 20 times that used previously. In 1972, Hounsfield (13) constructed the first practical (14) computerized tomographic scanner and reconstructed a tomographic image using a mathematical method developed by Cormack (15) in 1963. They were awarded the Nobel Prize in medicine in 1979. Subsequent developments in scanner technology decreased imaging time from several minutes to a few seconds. Developments in computerized tomography x-ray scanners led to three-dimensional (3-D) imaging instruments.

3.1. Theory and Equipment

The field of x-ray medical imaging can be divided into plane film and CT imaging. Plane film imaging produces projection images of an object placed between a source and a detector which in most cases is a sheet of photographic film (see Photography). CT imaging produces tomographic images of a transaxial slice through the body. CT utilizes a source of x-rays and an electronic detector which converts the x-radiation into an electrical signal. Many references on x-ray medical imaging are available (12–28).

X-rays are high energy photons falling into the wavelength, λ, and frequency, ν, ranges of $2.1 \times 10^{-11} < \lambda < 10^{-11}$ m and $1.5 \times 10^{19} < \nu < 2.9 \times 10^{19}$ s^{-1}, respectively. X-rays are produced by high speed electrons directed at a piece of metal. After collision between the electrons and the metal, the metal emits x-rays. The bombarding electrons interact with electrons in the innermost shells of the target metal. The interaction either promotes electrons to higher energy levels or ejects them completely from the metal atom. Relaxation of the electrons back into the vacant inner shell is accompanied by the emission of discrete high energy photons in the x-ray region of the electromagnetic spectrum. The specific wavelength emitted depends on the target metal and the energy of the electron. Other photons are given off when the high velocity electrons are decelerated as they pass through the metal target. This latter form of emission is continuous in nature and is referred to as Bremsstrahlung radiation.

The continuous and discrete emissions from an x-ray tube cover a broad range of frequencies. It is necessary to image using a narrow band of x-rays because the attenuation of x-rays by body tissues is frequency dependent. Narrowing the band of x-rays emanating from a source is accomplished by sending the beam through filters composed of aluminum, copper, or zirconium. This process is referred to as hardening of the beam.

X-ray vacuum tubes contain a resistively heated tungsten cathode (16). A negative potential (cathode) and a positive potential (anode) accelerate electrons from the cathode to a high velocity before collision with the tungsten anode. The geometry of the anode and cathode focus the beam of electrons in an area having approximate dimensions of 1×8 mm. Typical acceleration voltages range from 60 to 120 keV. The efficiency of x-ray generation by this technique is extremely low ($\sim$1%), therefore an enormous amount of heat is generated in the anode. To further complicate matters, the heat is concentrated in a small area of the anode where the electrons are focused. In some tubes this heat is dissipated by water or oil cooling the anode. Other tube designs incorporate a rotating anode which spreads the heat out over a larger mass of metal. The x-ray beam is typically pulsed rather than being a continuous wave (CW). Typical pulse widths are 1/4 to 1/30 of a second depending on the imaged anatomy.

X-rays interact with matter in three ways: photoelectric absorption, Compton scattering, and pair production. Photoelectric absorption is analogous to the absorption of visible light by an electron in an atom or molecule. The difference is that rather than adsorption taking place by an outer shell electron, x-ray absorption dislodges an inner electron from its orbital. Compton scattering involves the interaction of an x-ray with

a weakly bound electron. The interaction causes the x-ray to impart some of its energy to the electron in the form of kinetic energy and momentum. Pair production is an interaction between the nucleus of an atom and an x-ray which produces an electron–positron pair. Pair production occurs when the energy of the x-ray photon is $\geq 2\,mc^2 = 1.02$ MeV, where m is the mass of the photon and c the speed of light.

All three interactions occur when x-rays are absorbed by the human body. The first two dominate, however, owing to the lower energy of the x-rays. If N_0 x-ray photons incident on a tissue and N are transmitted, the absorbance, A, is proportional to the thickness, z, and linear attentuation coefficient μ, of the absorbing tissue.

$$A = \ln(N/N_0) = \mu z \qquad (1)$$

Some commonly encountered materials arranged in order of decreasing μ are lead $>$ $BaSO_4$ $>$ bone $>$ muscle $>$ blood $>$ liver $>$ fat $>$ air.

Several additional terms related to the absorption of x-radiation require definition: energy of a x-ray photon is properly represented in joules but more conveniently reported in eV; fluence is the sum of the energy in a unit area; intensity or flux is the fluence per unit time; and the exposure is a measure of the number of ions produced in a mass of gas. The unit of exposure in medicine is the Röntgen, R, defined as the quantity of radiation required to produce 2.58×10^{-4} C/kg of air. The absorbed dose for a tissue is a measure of energy dissipated per unit mass. The measure of absorbed dose most prevalent in the medical literature is the rad in the cm–gram–second system of dimensions. The International System of units for absorbed dose is the gray (Gy) which equals 1 J/kg. One rad is defined as the number of ergs absorbed per gram of tissue, or 0.01 J/kg.

Because of their short wavelength, x-rays are not conveniently focused using the principles of refraction, as are longer wavelength, ie, visible, photons. Therefore most imaging schemes utilize point sources of radiation. Images are projection or shadow images of the object placed between the source and the detector. Projection images assume x-ray photons travel a straight line from the source to the detector. Magnification of the imaged object can be achieved by placing the object further away from the screen. A problem associated with projection imaging is scattering of radiation as it interacts with matter. Scattered radiation contributes to intensity on the film in regions not along the original trajectory of the unscattered x-ray photon. A lead grid having a thickness approximately eight times the hole size is typically placed between the imaged object and the detector to minimize the detection of scattered radiation (17, 18). Such a grid is referred to as a Bucky diaphragm (Fig. 1).

3.1.1. Detectors

Two general types of detectors are used in x-ray medical imaging: scintillation and gas ionization. Scintillation detectors are used for both conventional projection and computerized tomographic imaging. Ionization detectors have been used only in CT applications. All detectors used in detection of x-ray radiation must be linear and have a maximum efficiency at the wavelength of the x-ray photon to be detected.

Scintillation detectors are substances which fluoresce when struck by x-radiation. Scintillation can, therefore, serve to convert x-ray photons into visible or ultraviolet light. Scintillation materials include thallium-activatedcrystals of sodium iodide, NaI(Tl), potassium iodide, KI(Tl), or cesium iodide, CsI(Tl); crystals of stilbene (α, β-diphenylethylene) [588-59-0] and anthracene [120-12-7], $C_{14}H_{10}$; bismuth germanium oxide [12233-56-6], $Bi_4Ge_3O_{12}$; barium fluoride [7787-32-8], BaF_2; calcium tungstate [7790-75-2], $CaWO_4$; barium lead sulfate, $BaSO_4$ and $PbSO_4$; zinc sulfide[7789-17-5], ZnS; and cadmium sulfide [1306-23-6], CdS. The application determines the specific material used, as do factors such as cost, durability, x-ray-to-visible light conversion efficiency, scintillation wavelength, transparency at scintillation wavelength, and x-ray attenuation coefficient. The visible or ultraviolet light from the scintillator is detected by photographic film (19, 20), electronic camera (21), or photomultiplier tube imaging systems (22) (see Photodetectors).

The imaging system responsible for the largest number of medical x-ray images utilizes photographic film. Direct exposure of film to x-rays results in an image, however, only 1% of the incident x-rays are absorbed by the emulsion. The use of double-sided emulsions doubles the sensitivity, but this is insufficient to produce

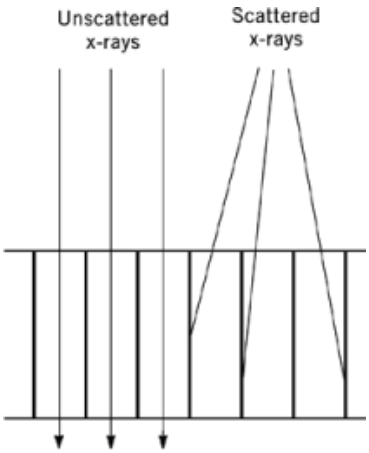

Fig. 1. Magnified view of a part of a lead Bucky diaphragm (grid) used to diminish scattered radiation from striking a detector. The grid is placed between the imaged object and the detector.

high quality images with a minimal dose of x-rays. Scintillators absorb approximately 10 to 70% of the x-rays and convert them to visible light, therefore scintillation materials are placed adjacent to photographic film to increase the efficiency of plane film x-ray imaging techniques. These scintillator plates are called intensifying screens (18, 23). The scintillation material and photographic film combination are chosen such that the wavelength of maximum sensitivity of the film matches that emitted by the scintillator. Intensifier screens are typically used on both sides of the film resulting in an overall sensitivity approximately 50 times greater than for the film alone. One drawback associated with intensifying screens is a blurring of the image. Intensifying screens are typically 50–500 μm in thickness. When an x-ray photon strikes the film, visible photons may be emitted in all directions. This emission pattern results in a blurring approximately equal to the thickness of the intensifying screen.

Whereas scintillation screens can be used to directly view x-rays passing through the body, the dose to a patient is too high. Instead, scintillation screens are combined with video cameras or electronic intensifier tubes and video cameras. This detection scheme is used in digital radiography where digital x-ray images are recorded, and fluoroscopy where temporal processes are to be followed.

Scintillators are also used in the detectors of CT scanners. Here an electronic detector, the photomultiplier tube, is used to produce an electrical signal from the visible and ultraviolet light photons. These imaging systems typically need fast scintillators with a high efficiency.

A gas ionization detector consists of a tube filled with a high pressure gas and two electrodes. A tube filled with 2 MPa (20 atm) of xenon is common. The gas in the tube ionizes when x-rays pass through the tube causing a current to flow between a high voltage potential placed across the electrodes. This concept is similar to that used in a Geiger tube detector. Gas ionization detectors are utilized in some CT scanners.

3.1.2. Computerized Tomography

Computerized tomography (CT) imaging is based on obtaining a series of one-dimensional (1-D) projection x-ray images which encompass 180° of projection angles with respect to the imaged object. Each 1-D projection represents the absorption of x-ray radiation along the line from the source to the detector. The 1-D projection images are back-projected using computer programs to produce an image of the internal contents of the original object. The mathematics that describe the signal-generating process in CT imaging are called the Radon and inverse Radon transforms (24). The Radon transform describes the collection of projection functions $P_\theta(t)$ from

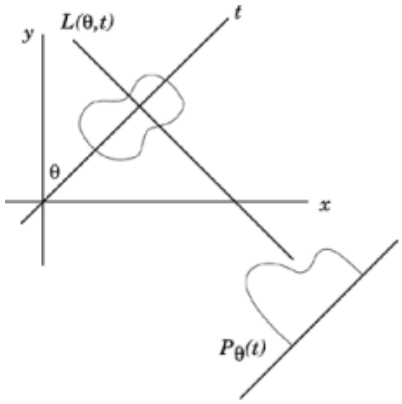

Fig. 2. Description of the functions represented in the mathematical definition of the Radon and inverse Radon transforms. See text.

an object *f(x,y)*. The Radon transform of *f(x,y)* is

$$P_\theta(t) = \int_{L(\theta,t)} f(x, y)\, ds \qquad (2)$$

where the line $L(\theta,t)$ is defined by Figure 2. The integration at values of θ and t is performed along line$L(\theta,t)$. $P_\theta(t)$ is the projection of function *f(x,y)* onto line t where θ is the angle between t and the y-axis. The inverse Radon transform describes the back-projection of the Radon transform of an object to obtain an image of the original object. The inverse Radon transform is

$$f(x, y) = \int_0^\pi P_\theta(t)\, d\theta \qquad (3)$$

where the integration is over projection angles between zero and 180°.

The first scanner consisted of an x-ray tube and single-detector combination which moved in unison along the object being imaged (13). In addition to this translational motion, the source/detector assembly was rotated 360° about the imaged object in one-degree steps. At each step the source/detector assembly scanned across the object. The projection images at each step were used to reconstruct a tomographic image of the object. Second generation scanners used a small-angle fan-beam source of x-rays and a detector array. The source and detector array still underwent the translational motion to record the 1-D projection data, but because the array of detectors recorded more information than single-point detectors, fewer rotational steps were required to produce an image. Third generation systems use a wider detector array and an x-ray source having a 30° beam. As a consequence, projection data from the entire object can be recorded at one instant without the need for the translational motion. Additionally, the rotational motion can be performed more quickly and the x-ray source can be pulsed rather than continuous wave. Fourth generation detectors utilize a stationary 360° ring of detectors and a rotating x-ray source having a 30° spread. Experimental scanners are being developed with more sources and detectors which allow dynamic x-ray CT imaging of a beating heart (25). A 3-D image of an object may be obtained by moving either the patient or the source/detector gantry axially with respect to each other. To minimize the x-ray exposure to the patient, two-dimensional (2-D) detector arrays are being used which also eliminate the need for axial motion of the object.

3.2. Applications

Applications of x-ray imaging span the entire discipline of medicine. Some of the more common applications are angiography, mammography, and GI, muscular skeletal, neuro, and dental imaging. Muscular skeletal imaging primarily utilizes plane film x-ray imaging. A common use is in gathering the information necessary to set broken bones. Other nonplane film procedures for muscular skeletal imaging are bone density measurements utilizing dual energy CT scans.

Angiography is the study of the blood vessels of the human body. X-ray images possess poor contrast between blood and tissues. As a consequence a contrast agent is typically introduced into the circulatory system to provide the necessary contrast. One of the first angiograms was performed in 1986 using an amputated hand and a mercuric sulfide [1344-48-5] containing contrast agent (12). Fortunately less invasive and safer protocols are available. Angiographic contrast agents generally contain iodine. These agents are usually retained by the body for less than 24 hours. One such contrast agent is *N*,*N*′-bis(2,3-dihydroxypropyl)-5-[*N*-(2,3-dihydroxypropyl)-acetamido]-2,4,6-triiodoisophthalamide [66108-95-0], $C_{19}H_{26}I_3N_3O_9$, known as iohexol.

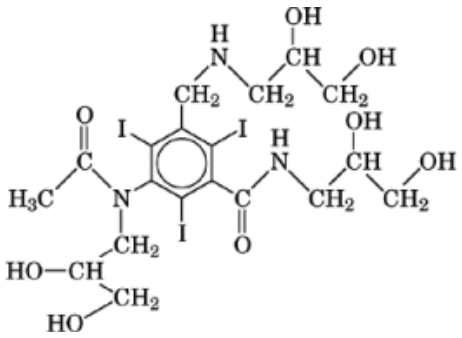

X-ray mammograms are one component of a strategy for lowering a woman's risk of dying from breast cancer. Microcalcification is usually associated with some breast lesions and can be imaged with x-rays. The breast is compressed between two parallel plates and a projection image obtained. Early mammograms were made using industrial x-ray film. As of this writing mammography systems utilize intensifier screens, grids, and high speed film. The x-ray energy is typically 50 keV. One of the shortfalls of mammography is that lesions are not readily detected in dense breasts, that is breasts which are predominantly parenchymal tissue. The overall false negative rate for finding breast cancer by x-ray mammography is 15% for all women, and 40% for women with dense breasts (26, 27).

Gastrointestinal x-ray imaging is the imaging of the small and large intestines and the colon. The contrast between the various tissues found in the abdomen is poor. As a consequence, a contrast agent is introduced into the digestive tract which absorbs more x-rays than do the tissues in the abdomen. A common contrast agent is barium sulfate [7727-43-7], although iodinated compounds have been used. Owing to the much higher linear attenuation coefficient of the contrast agent, a higher (120 keV) energy x-ray typically is used.

Neuro imaging focuses on the brain and spine and is primarily performed using CT scanning technology. Neuro imaging is often performed with the aid of contrast agents having an affinity for certain types of tissues in the brain. Typical contrast agents are gadolinium-based compounds that possess a higher linear attenuation coefficient than soft tissues.

Dental x-rays provide valuable information on the health of teeth which cannot be obtained by any other medical imaging modality. Dental x-ray procedures use a piece of film placed in the mouth between the tongue and the teeth. A 60 to 70 keV source of x-rays, located outside the mouth, is directed at the film. Metal fillings attenuate x-rays striking the film and therefore appear white in a projection image. Tooth decay appears dark as it attenuates x-rays less than normal tooth enamel.

Table 1. Specific Organ Doses from X-Ray Procedures[a]

	Organ or tissue dose, μGy[b]u				
Procedure	Thyroid	Marrow	Breast	Lung	Ovaries
angiogram, carotid	3,000	15,000			
barium enema		3,000			7,900
chest x-ray			140	200	
CT					
brain	960	1,400			
upper abdomen	540	1,700	1,480	6,800	
lower abdomen		2,600	210	1,130	9,500
dental x-ray					
intraoral	10	25			
pantomography		70	50		
mammogram			1,000		
rib x-ray			4,100	3,000	
upper GI tract x-ray		1,200		5,000	

[a]Ref. 21.
[b]To convert μmGy to rads, multiply by 1.0×10^{-4}.

3.3. Safety

X-rays are classified as ionizing radiation. These photons possess sufficient energy to ionize molecules leading to bond breakage and the formation of free radicals. There has been increasing concern about the safety of x-ray medical imaging since the 1970s. The most significant concern centers on radiation dose obtained in x-ray imaging session. In addition to the short-term effects of the radiation, there also is concern about the long-term effects. For example, the abdomen of a premenopausal woman is rarely imaged because of potential damage to the ovaries. Significant advances have been made in decreasing the exposure from x-rays during a plane film imaging session. Radiation exposure during plane film imaging decreased approximately 20-fold from 1960 to 1994. Radiation exposure from CT imaging has, however, increased by a factor of two to three since the first generation CT scanners (28). Table 1 lists the approximate dose obtained from various x-ray imaging procedures to specific body tissues.

An ancillary concern arises from the use of contrast agents, eg, gadolinium complexes during CT scans, barium for GI images, and iodine complexes during angiography. Much research has gone into complexing gadolinium, barium, or iodine to minimize health risks. Despite these efforts, health risks from the use of contrast agents cannot be trivialized. Moreover, most individuals being imaged are already ill and some of the contrast agents are difficult for their bodies to handle. The information gained from a medical imaging procedure must always be balanced against health risks of imaging procedure.

All x-ray equipment must be periodically inspected and the output monitored and calibrated to minimize the chance of accidental overexposure. Another concern involves radiation accumulation by medical personnel operating x-ray equipment. Although the dose to any one patient may be low, the accumulated dose to a clinician performing multiple exams each day over the course of a year is great. Therefore, personnel working with x-ray equipment must take precautions constantly to minimize and monitor exposure. Lead aprons and film badges are used to minimize exposure and to monitor accumulated dose, respectively.

4. Ultrasound Imaging

Sound waves having a frequency above 20 kHz, which were audible to a dog but not to humans, were discovered in 1876 (29) and referred to as ultrasound waves. The piezoelectric effect, discovered in 1880 by Jacques and

Table 2. Ultrasound Properties of Human Tissues[a]

Tissue	υ, m/s	Attenuation coefficient, α, at 1 MHz, dB/cm
air	331	
adipose	1450	0.63
water	1480	
humor		
aqueous	1500	0.1
vitreous	1520	0.1
brain	1541	0.85
liver	1541	0.94
spleen	1566	
kidney	1561	1.0
blood	1575	0.18
muscle	1550–1625	1.3–3.3
eye lens	1620	
cartilage	1655	
tendon	1750	
skull bone	4080	20

[a]Refs. 36 and 37.

Pierre Curie (30), and the reverse effect discovered one year later, opened the way for the production and detection of high frequency ultrasound waves (31). After the development of sonar technology in the 1940s, medical ultrasound imaging began in the early 1950s. Soft tissues in the body were imaged in 1952 (32), lesions were shown to be identifiable in 1954 (33), and the precursor of the first clinical ultrasound imager was developed in 1958 (34). Advances in ultrasound hardware and clinical applications occurred throughout the 1960s and 1970s making medical ultrasound imaging an indispensable, inexpensive, and respectable medical imaging modality. More recent advances in ultrasound research have led to the development of Doppler ultrasound imaging of blood flow (35).

4.1. Theory

Ultrasound medical imaging is performed by sending a pulse of ultrasound energy into the body and listening for reflections or echoes. This procedure is similar to that used to estimate the distance across a canyon by measuring the time for sound to travel across the canyon and back. Just as sound waves in air have a characteristic speed or propagation constant, ultrasound waves have a characteristic propagation constant in tissue. The propagation rate, υ, in an average soft tissue is 1540 m/s. Values for a few specific tissues can be found in Table 2. Boundaries between tissues having different propagation contants reflect ultrasound, just as the walls of the canyon reflect sound waves. The time, τ, between an ultrasound pulse and a reflection is an indication of the thickness of a tissue. The distance, z, from the source to the boundary is

$$z = \upsilon\tau/2 \qquad (4)$$

For example, an echo detected 13 μs after the ultrasound pulse represents a boundary 10 cm away from the source.

For ultrasound technology to be useful in medicine, a method is needed for creating an image from the reflected ultrasound energy. When measuring distance between canyon walls, the average distance is determined because of variations in the wall distance. Sending out a focused beam of sound gives a more accurate measurement of distance relative to the focal point of the sound. Similarly, in ultrasound medical imaging the distance between an ultrasound source and a tissue boundary is best determined using a focused

beam of ultrasound waves. This 1-D image is not, however, very useful for clinical purposes. A 2-D image is necessary to provide relevant information.

Ultrasound images are typically tomographic images with a slice thickness of 1–2 mm and a field of view of 20–30 cm. A tomographic ultrasound image is generated by sending a series of ultrasound pulses into the portion of anatomy being imaged. Each ultrasound pulse is sent out at a different angle from the source so as to sweep through the anatomy to be imaged in a manner similar to radar sweeping across the sky for airplanes. There are various methods of sweeping the ultrasound beam across the imaged plane.

The source and detector of ultrasound in an ultrasound medical imager is called a transducer. The transducer is a piezoelectric crystal which physically changes its dimensions when a potential is applied across the crystal (38). The application of a force to the piezoelectric crystal which changes its dimensions creates a voltage in the crystal. Application of an oscillating potential to the crystal causes the dimensions of the crystal to oscillate and hence create a sound at the frequency of the oscillation. The application of an oscillating force to the crystal creates an alternating potential in the crystal.

Typical piezoelectric materials are ceramic crystals and copolymers, such as poly(vinylidene fluoride-*co*-trifluoroethylene), $(—CH_2—Cl_2—)_n—(—CF_2—CFH—)_m$ (39). Ceramic crystals have a higher piezoelectric efficiency. Their high acoustic impedance compared to body tissues necessitates impedance matching layers between the piezoelectric and the tissue. These layers are similar in function to the antireflective coatings on a lens. Polymer piezoelectric materials possess a more favorable impedance relative to body tissues but have poorer performance characteristics. Newer transducer materials are piezoelectric composites containing ceramic crystals embedded in a polymer matrix .

The required sweeping of the ultrasound beam across the imaged plane may be accomplished by one of three methods. The transducer may be physically moved through a series of angles to obtain the image, the transducer may be pointed at an ultrasound mirror that rotates through the desired angles, or a linear array of transducers may be employed (40). Each element in the array of transducers is fired at a different time so as to focus the beam of ultrasound at the desired angle. Although smaller arrays are used, typical arrays are approximately 10 cm in length and may contain as many as 300 elements.

The transducers on most ultrasound imaging systems operate at a frequency between 1 and 20 MHz. The attenuation, A, of ultrasound by tissues is both frequency and tissue dependent. The attenuation coefficient, α, of a tissue is defined by equation 5:

$$A = 10 \log(P/P_0) = \alpha f z_i \qquad (5)$$

where P is the power of an ultrasound wave of frequency f and initial power P_0 after traversing a distance z_i in tissue i. Typical values of α for various biological tissues are found in Table 2. The frequency dependence of the ultrasound attenuation allows the ultrasound imager to select the depth to image. Higher frequencies are used to view shorter distances from the transducer. The tissue dependency of the attenuation opens up the possibility of tissue classification using ultrasound intensities.

The resolution in an ultrasound image is, among other things, related to the duration of the ultrasound pulse, ie, the shorter the pulse the better the resolution. Imaging may not be performed when the pulse duration is longer than the time to receive an echo. The shorter the ultrasound pulse the more difficult it is to discern it from noise, and the poorer the SNR of the image. As the pulse duration is decreased, the power of the ultrasound pulse is typically increased to compensate for the poorer SNR.

Another factor affecting the SNR in an ultrasound image is interference between reflected signals from small scatters in the tissues. The ultrasound signals reflected from small reflecting spots in the tissues can constructively and destructively interfere causing a speckle pattern in the image. This speckle pattern manifests itself as a degradation in the SNR of the images.

Contrast in an ultrasound image is related to differences in propagation constants for the tissues. A boundary between two tissues having a large difference in propagation constant reflects large amounts of

ultrasound. Ultrasound contrast agents are substances that are introduced into a tissue to change the propagation constant and hence reflect more ultrasound energy (41, 42). Typical ultrasound contrast agents are lipid-stabilized microbubbles having a diameter of 1–5 micrometers.

4.2. Applications

Ultrasound imaging is used for imaging of soft tissues. Its primary advantages are low cost and safety compared to other medical imaging modalities. Ultrasound imaging finds its greatest applications in obstetrics and gynecology for studying the uterus and a fetus, in cardiology for studying the function of the heart, and for imaging of the abdomen.

Ultrasound energy reflected from a tissue contains both amplitude and frequency information. Generally only the amplitude information is utilized to create an image. The frequency information, typically discarded, contains information on the velocity of the tissues. Doppler ultrasound uses this frequency information. The velocity of blood flowing through the veins and arteries of the body (35) is obtained using the Doppler effect. Blood flowing toward the transducer reflects higher frequency ultrasound than in the incident pulse; blood flowing away from the transducer reflects lower frequency ultrasound waves. This frequency information is typically processed and presented as pseudo-color overlaid on top of a conventional ultrasound image.

Special small ultrasound transducers, often referred to as endoscopic transducers, have been designed which can be inserted into blood vessels to examine blockages in arteries (43). These transducers operate at approximately 20 MHz and have a viewing distance of less than a centimeter. Such devices are capable of producing ultrasound images of the inside of arteries and veins. The quality of the ultrasound image is sufficient to determine the type of blockage.

4.3. Safety

High power ultrasound waves can cause local heating and transient cavitation in water (44). Transient cavitation is a process in which microscopic gas bubbles expand and collapse as a consequence of the ultrasound wave. The rapid collapse can be adiabatic causing the energy to be transferred to bond-breaking processes that create free radicals and give rise to the health concern (45, 46). Typical ultrasound contrast agents are lipid-stabilized microbubbles having a diameter of 1–5 micrometers. These microbubbles, when exposed to ultrasound, may behave the same way as the ultrasound-generated bubbles and create transient free radicals. The difference in using the contrast media is that the concentration of free radicals is much higher because of the introduced bubbles. The rule of thumb in ultrasound medical imaging is to utilize a power level that is as low as reasonably possible.

5. Magnetic Resonance Imaging

As of this writing, magnetic resonance imaging (MRI) is the newest medical imaging technique available (47–49). The technique upon which MRI is based, nuclear magnetic resonance (nmr), was developed independently in the 1940s by Bloch and Purcell (see Magnetic spin resonance). In the 1950s and 1960s nmr was used extensively for chemical and physical analysis. In the 1970s several developments occurred which initiated the development of MRI. The first was the discovery that an nmr property of tissues called the spin-lattice relaxation time could be used to distinguish between a tumor and healthy tissue (50). Another factor was the implementation of x-ray-based computed tomography in a clinical setting, showing that hospitals were willing to purchase expensive equipment vital for a diagnosis. A third development was the demonstration of imaging using nmr and the CT back-projection technique (51). The final development which allowed MRI to become viable was the development of phase and frequency encoding the MRI (52).

Table 3. Gyromagnetic Ratios for Biologically Relevant Nuclei[a]

Nuclei	γ, MHz/T[b]	Natural abundance, %
^{1}H	42.58	99.99
^{13}C	10.71	1.108
^{14}N	3.08	99.63
^{23}Na	11.27	100
^{25}Mg	2.61	10.13
^{31}P	17.25	100
^{35}Cl	4.17	75.53
^{39}K	1.99	93.10
^{43}Ca	2.86	0.13

[a]Ref. 56.
[b]To convert T to Gauss, multiply by 1.0×10^4

The 1980s saw the first demonstration of a whole body imager and the first commercially available magnetic resonance imagers. Additionally, development of rapid imaging sequences pushed the imaging time for a single image from five minutes in 1982 to five seconds in 1986, and to video rates in 1989. Resolution on nmr microscopes was pushed to approximately 10 μm. Magnetic resonance angiography was developed in the late 1980s. The 1990s saw the awarding of the Nobel Prize in chemistry to Richard Ernst for his contributions to pulsed nmr and MRI. The most recent development was the discovery in 1993 that echo planar MRI could be used for functional imaging of the brain.

5.1. Theory and Equipment

MRI is conceptually more difficult to understand than other medical imaging modalities because it is not based on simple optical principles of absorption and reflection of electromagnetic radiation. MRI is based on the principles of nmr, therefore any description of the principles of MRI should be preceded by a good understanding of nmr. This fact makes MRI very interesting to chemists. A brief review of the nmr is presented herein. The less knowledgeable reader is directed to the entry on magnetic spectroscopies (see Magnetic spin resonance) or one of the many references for a more detailed description (53–55).

5.1.1. Nuclear Magnetic Resonance

Nuclear magnetic resonance is based on a property of the atomic nucleus called spin which can be thought of as a simple magnetic moment. When a nucleus with spin is placed in an external magnetic field, the magnetic moment can take on one of two possible orientations, one low energy orientation aligned with the field and one high energy orientation opposing the field. A photon with an energy equal to the energy difference between the two orientations or states can cause a transition between the states. The greater the magnetic field the greater the energy difference and hence the frequency of the absorbed photon. The relationship between the applied magnetic field B_0 and the frequency of the absorbed photon ν is linear.

$$\nu = \gamma B_0 \qquad (6)$$

The proportionality constant γ is called the gyromagnetic ratio which is a function of the magnitude of the nuclear magnetic moment. Therefore each isotope having a net nuclear spin possesses a unique γ. The γ of some biologically relevant nuclei can be found in Table 3.

The remainder of the nmr description adopts a macroscopic perspective of the spin system in which the B_0 field is applied along the z-axis. Groups of nuclei experiencing the same B_0 are called spin packets. When placed in a B_0 field, spin packets precess about the direction of B_0 just as a spinning top on earth precesses

about the direction of the gravitational field. The precessional frequency, also called the Larmor frequency, ω, is equal to $2\pi\nu$. The direction of the precession is clockwise about B_0, and the symbol ω_0 is reserved for spin packets experiencing exactly B_0. It is often helpful in nmr and MRI to adopt a rotating frame of reference to describe the motion of magnetization vectors. This frame of reference rotates about the z-axis at ω_0. The axes in the rotating frame of reference are referred to as z, x', and y'.

An nmr sample contains millions of spin packets, each having a slightly different Larmor frequency. The magnetization vectors from all these spin packets form a cone of magnetization around the z-axis. At equilibrium, the net magnetization vector M from all the spins in a sample lies in the center of the cone along the z-axis. Therefore the longitudinal magnetization M_z equals M and the transverse magnetization M_{xy} equals zero at equilibrium. Net magnetization, perturbed from its equilibrium position, wants to return to its equilibrium position. This process is called spin relaxation.

The return of the z component of magnetization to its equilibrium value is called spin-lattice relaxation. The time constant which describes the exponential rate at which M_z returns to its equilibrium value M_{z0} is called the spin-lattice relaxation time, T_1. Spin-lattice relaxation is caused by time-varying magnetic fields at the Larmor frequency. These variations cause transitions between the spin states and hence change M_z. Time-varying fields are caused by the random rotational and translational motions of the molecules in the sample possessing a magnetic moment. The frequency distribution of random motions in a liquid varies with temperature and viscosity. In general, relaxation times tend to get longer as B_0 and ν increase because there are fewer relaxation-causing frequency components present in the random motions of the molecules as ν increases.

At equilibrium, the transverse magnetization M_{xy} equals zero. A net magnetization vector rotated off the z-axis creates transverse magnetization. This transverse magnetization decays exponentially with a time constant called the spin–spin relaxation time T_2 Spin–spin relaxation is caused by fluctuating magnetic fields which perturb the energy levels of the spin states and dephase the transverse magnetization. T_2 is inversely proportional to the number of molecular motions less than and equal to the Larmor frequency. T Eqn$_2$ has two components: a pure T_2 resulting from molecular interactions, and one resulting from spatial inhomogeneities in the B_0 field. The overall T_* (referred to as T_2 star) is defined as

$$1/T_2^* = 1/T_2 + 1/T_{2_{\text{inhomogeneous}}} \qquad (7)$$

In pulsed nmr and MRI, radio-frequency (r-f) energy is put into a spin system by sending rf into a resonant LC circuit, the inductor of which is placed around the sample. The inductor must be oriented with respect to the B_0 magnetic field so that the oscillating r-f field created by the rf flowing through the inductor is perpendicular to B_0. The r-f magnetic field is called the B_1 magnetic field. When the r-f inductor, or coil as it is more often called, is placed around the x-axis, the B_1 field oscillates back and forth along the $\pm$ x-axis.

In pulsed nmr spectroscopy, it is the B_1 field which is pulsed. Turning on a B_1 field for a period of time τ causes the net magnetization vector to precess in ever widening circles around the z-axis. Eventually, the vector reaches the xy plane. If B_1 is left on longer, the net magnetization vector reaches the negative z-axis. In the rotating frame of reference, this vector appears to rotate away from the z-axis. The rotation angle θ, which is measured clockwise about the direction of B_1 in radians, is proportional to γ, B_1, and τ.

$$\theta = 2\pi\gamma B_1\tau \qquad (8)$$

Any transverse magnetization M_{xy} precesses about the direction of B_0. An nmr signal is generated from transverse magnetization rotating about the z-axis. This magnetization reduces a current in a coil of wire placed around the x- or y-axis. As long as there is transverse magnetization changing with respect to time, there is an induced current in the coil. For a group of nuclei having one identical chemical shift, the signal is an exponentially decaying sine wave which decays with a time constant T^*_2. It is predominantly the inhomogeneities in B_0 which cause the spin packets to dephase. Net magnetization which has been rotated away

from its equilibrium position along the z-axis by exactly 180° does not create transverse magnetization and hence does not give a signal. The time-domain signal from a net magnetization vector in the xy plane is called a free induction decay (FID). This time domain signal must be converted to a frequency domain spectrum to be interpreted for chemical information. The conversion is performed using a Fourier transform. The hardware in most nmr spectrometers and magnetic resonance imagers detects both M_x and M_y simultaneously. This detection scheme is called quadrature detection. These two signals are equivalent to the real and imaginary signals, therefore the input to the Fourier transform is complex. Sampling theory dictates that digitization of the FID at frequency f complex points per second gives a spectrum of frequency width f.

In pulsed Fourier transform nmr spectroscopy, short bursts of r-f energy are applied to a spin system to induce a particular signal from the spins within a sample. A pulse sequence is a description of the types of r-f pulses used and the response of the magnetization to the pulses. The simplest and most widely used pulse sequence for routine nmr spectroscopy is the 90-FID pulse sequence. As the name implies, the pulse sequence is a 90° pulse followed by the acquisition of the FID. The net magnetization vector, which at equilibrium is along the positive z-axis, is rotated by 90° down into the xy plane. The rotation is accomplished by choosing an r-f pulse width and amplitude so that the rotation equation for a 90° pulse is satisfied. At this time the net magnetization begins to precess about the direction of the applied magnetic field B_0. Assuming $T_2^* < T_1$, the net magnetization vector begins to dephase as the vectors from the individual spin packets in the sample precess at their own Larmor frequencies. Eventually, M_{xy} equals zero and the net magnetization returns to its equilibrium value along z. The signal which is detected by the spectrometer is the decay of the transverse magnetization as a function of time. The FID or time domain signal is Fourier transformed to yield the frequency domain nmr spectrum.

5.1.2. Magnetic Resonance Imaging

Magnetic resonance imaging (MRI) is a tomographic imaging modality. The basis of MRI, equation 6, states that the resonance frequency of a nucleus is proportional to the magnetic field it is experiencing. If a spatially varying magnetic field is set up across a sample, the nuclei within the sample resonate at a frequency related to their positions. For example, if a 1-D linear magnetic field gradient G_z is set up in the B_0 field along the z-axis, the resonant frequency ν is defined by

$$\nu = \gamma(B_0 + zG_z) \qquad (9)$$

The origin of the xyz coordinate system is the point in the magnet where the field is exactly equal to B_0 and spins resonate at ν_0. This point is referred to as the isocenter of the magnet. Equation 9 explains how a simple 1-D imaging experiment can be performed. The sample to be imaged is placed in a magnetic field B_0. A 90° pulse of r-f energy is applied to rotate magnetization into the xy plane. A 1-D linear magnetic field gradient G_z is turned on after the r-f pulse and the FID is immediately recorded. The Fourier transform of the FID yields a frequency spectrum that can be converted to a spatial, z, spectrum as shown in equation 10:

$$z = (\nu - \nu_0)/\gamma G_z \qquad (10)$$

This simple concept of a 1-D image can be expanded to a 2-D image employing back-projection technology similar to that used in CT imaging (51). If a series of 1-D images, or projections of the signal in a sample, are recorded for linear 1-D magnetic field gradients applied along several different trajectories in a plane, the spectra can be transformed into a 2-D image using an inverse Radon transform (24) or a back-projection algorithm. This procedure is seldom used. Instead, Fourier-based imaging techniques are used in most MRI (52, 57).

A Fourier-based imaging technique collects data from the k-space (2-D Fourier transform of the image) of the imaged object. Figure 3 depicts a timing diagram for a Fourier imaging sequence using simple 90-FID

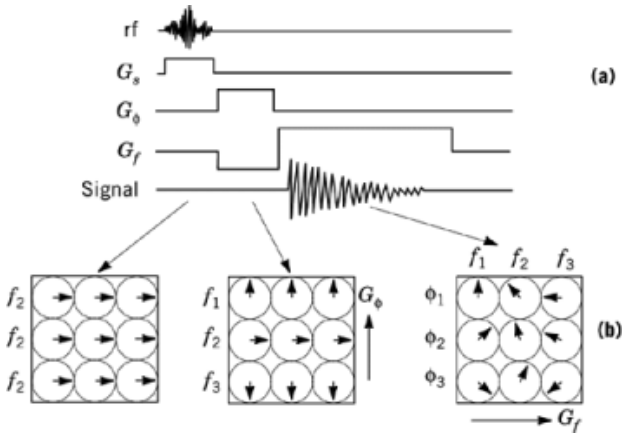

Fig. 3. Timing diagram with corresponding magnetization vector presentation for a 90-FID imaging sequence: (**a**) timing diagram which depicts the time during which the rf, G_s, G_π, and G_f are applied and the signal is acquired; (**b**) vector diagram describing the evolution of nine magnetization vectors during the sequence. See text.

sequence. The timing diagram describes the application of rf and three magnetic field gradients called the slice selection (G_s), phase encoding (G_π), and frequency encoding (G_f) gradients. The first step in the Fourier imaging procedure is slice selection of those spins in the object for which the image is to be generated. Slice selection is accomplished by the application of a magnetic field gradient at the same time the r-f pulse is applied. A r-f pulse, having frequency width $\Delta\nu$ centered at ν, excites when applied in conjunction with a field gradient G_z, spins centered at $z = (\nu - \nu_0)/\gamma G_z$ with a spread of spins at z values $\Delta z = \Delta\nu/\gamma G_z$. Spins experiencing a magnetic field strength not satisfying the resonance condition are not rotated by the r-f pulses, and hence slice selection is accomplished. The image slice thickness is given by Δz. For a clean slice, ie, all spins along the slice thickness are rotated by the prescribed rotations, the frequency content of the pulse must be equal to a rectangular-shaped function. Therefore, the r-f pulse must be shaped as a sinc ($\sin x/x$) function in the time domain.

The next step in the Fourier imaging procedure is to encode some property of the spins as to the location in the selected plane. Spins could easily be encoded as to their x position by applying a gradient G_x after the r-f pulse and during the acquisition of the FID. The difficulty is in encoding the spins with information as to their y location. This is accomplished by encoding the phase of the precessing spin packets with y position (see Fig. 3). Phase encoding is accomplished by turning on a gradient in the y direction immediately after the slice selection gradient is turned off and before the frequency-encoding gradient is turned on. The spins in the excited plane now precess at a frequency dependent on the y position. After a period of time τ the gradient is turned off and the spins have acquired a phase π equal to

$$\phi = 2\pi\gamma\tau y G_y \qquad (11)$$

Figure 3 describes for nine magnetization vectors the effect of the application of a phase-encoding gradient, G_y, and a frequency-encoding gradient, G_x. The phase-encoding gradient assigns each y position a unique phase. The frequency-encoding gradient assigns each x position a unique frequency. If the phase and frequency of a spin packet could be assessed independently, its position could be assigned in the xy plane. Unfortunately, this cannot be accomplished with a single pulse and signal. The phase-encoding gradient must be varied in amplitude so a 2π radian phase variation between the isocenter and the first resolvable point in the y direction can be achieved, as well as a 256 π radian variation from center to edge of the imaged space for 256-pixel

resolution in the phase-encoding direction. The result is to traverse, line by line, the k-space of the image. The negative lobe on the frequency-encoding gradient (see Fig. 3), which was not previously described, shifts the center of k-space to the center of the signal acquisition window.

The B_0 field is created by a large-diameter solenoidal-shaped superconducting magnet. The gradient fields are created by room temperature gradient coils located within the bore of the magnet. These coils are driven by high current audio frequency amplifiers. The B_1 field is introduced into the patient by means of a large LC circuit which surrounds the anatomy to be imaged (58). The same or a separate LC circuit is used to detect the signals from the precessing spins in the body.

The field of view (FOV) is dependent on the quadrature sampling rate, T_s, during the application of G_f, and the magnitude of G_f.

$$\text{FOV} = R_s/\gamma G_f \qquad (12)$$

The 2-D k-space data set is Fourier transformed, and the magnitude image generated from the real and imaginary outputs of the Fourier transform.

In routine clinical imaging the thickness of a slice is approximately 3 mm and the in-plane resolution approximately 0.8 mm for a 20-cm FOV, 256×256 pixel image. The volume of a voxel is, therefore, approximately two mm 3. That is, taking into account the size of organs and composition of tissues in the body, a voxel is often comprised of more than one substance. As a consequence, the nmr signal from a voxel is a summation of the nmr signals from the substances found in the voxel. Any variation in the signal resulting from the relative amounts of the components found in a voxel is referred to as a partial volume effect.

The most abundant spin-bearing nucleus in the human body is hydrogen. The two most abundant forms of hydrogen are fat and water hydrogens. These hydrogens yield one signal in the image, as chemical shift and spin–spin splitting information is generally not utilized. Occasionally the different chemical shifts for water and fat hydrogens can lead to an artifact in an image called a chemical shift artifact. Hydrogens associated with proteins and the other building blocks of tissues have very short T_2 value and do not contribute directly to the signal. Magnetic resonance images have also been recorded for sodium and phosphorus.

A problematic artifact associated with MRI arises when the imaged subject moves during acquisition of the k-space data. Such motion may result in a discontinuity in the frequency-encoded or phase-encoding direction data of k-space. When Fourier transformed, such a discontinuity causes a blurred band across the image corresponding to the object that moved. Such an artifact in an image is referred to as a motion artifact.

In Figure 3, the slice selection gradient is applied along the z-axis and the phase and frequency encoding gradients along the y and x axes, respectively. In practice the gradients can be applied along any three orthogonal axes, the only restrictions being that the slice selection gradient be perpendicular to the imaged plane.

The most routinely used imaging sequence is the spin-echo. Its popularity is attributable to its ability to produce images which display variations in T_1, T_2, and spin density, ρ, of tissues. This sequence consists of 90° and 180° r-f pulses repeated every TR (repetition time of the sequence) seconds. These pulses are applied in conjunction with the slice selection gradients. The phase-encoding gradient is applied between the 90° and 180° pulses. The frequency-encoding gradient is turned on during the acquisition of the signal. The signal is referred to as an echo because it comes about from the refocusing of the transverse magnetization at an echo time (TE) after the application of the 90° pulse. The signal from a voxel in the body is equal to a summation over all the different types of spins, i, in the voxel.

$$S = \sum_i \rho_i (1 - e^{-\text{TR}/T_{1i}}) e^{-\text{TE}/T_{2i}} \qquad (13)$$

The goal of the MRI scientist is to maximize the contrast-to-noise ratio between tissues. Examination of equation 13 reveals that by varying TR and TE, the clinician has a tremendous amount of flexibility to select the desired contrast between two tissues.

The contrast between any two tissues may be maximized by prudent choice of the imaging parameters. Clinicians have adopted nomenclature for the various types of images produced as a consequence of the choice of imaging parameters. A T_1-weighted image is one in which image contrast displays differences in T_1 of the tissues. A spin-echo sequence produces a T_1-weighted image when $\mathrm{TR} \leq T_1$ and $\mathrm{TE} < T_2$. A T_2-weighted image is one in which contrast between the tissues is primarily because of differences in T_2 of the tissues. A spin-echo sequence produces a T_2-weighted image when $\mathrm{TR} > T_1$ and $\mathrm{TE} \geq T_2$. Spin density weighting is, as expected, an image where contrast displays differences in spin density of the tissues. A spin-echo sequence produces a ρ-weighted image when $\mathrm{TR} > T_1$ and $\mathrm{TE} < T_2$.

The clinician may also change the contrast in an image using a chemical contrast agent (59). A contrast agent is typically a paramagnetic substance that is introduced into the body and has an affinity for certain tissue types. When a contrast agent comes in contact with the tissue, it changes the T_1 and T_2 of the tissue. The magnetic resonance signals from those tissues can, therefore, be altered relative to other tissues with a lesser affinity to the contrast agent. Typical MRI contrast agents contain gadolinium. The gadolinium is chelated with a ligand such as ethylenediaminetetraacetic acid [60-00-4] (EDTA), diethylenetriaminepentaacetic acid [67-43-6] (DTPA), or tetraazacyclododecanetetraacetic acid [60239-18-1] (DOTA) to lower its toxicity.

5.2. Applications

Magnetic resonance imaging finds its greatest use in neuro imaging (60). MRI has excellent soft tissue specificity and can, therefore, be used to identify many types of lesions in the brain and spinal cord. The utility of MRI in providing structural information about these areas has surpassed that of CT. In addition to the structural information, MRI can also provide functional information (61, 62). Previously, functional imaging required the use of positron emission tomography (PET).

Brain functional imaging using MRI is based on the fact that during brain activity the flow of blood to the region of activity increases. This in turn causes a change in the contrast between regions with activity and those without. Because this change occurs in fractions of a second, the imaging of an entire slice through the brain must be performed in a period of time less than this. The technique which allows this is called echo planar imaging. An echo planar imaging sequence allows images to be recorded at video rates, ie, 1/15 to 1/30 second. The faster image acquisition rate is the result of traversing all k-space for an image during a single echo. The frequency-encoding gradient is rapidly switched between a positive and negative value while the phase-encoding gradient is pulsed at each switching of G_f. This procedure permits the rastering through k-space at video rates.

The second largest application of MRI is in muscular skeletal imaging (63) of joints such as the knee, shoulder, hips, and wrist. Torn ligaments and rips in the cartilage between the tibia and femur are readily seen using MRI. This method is preferred by the patient over arthroscopic imaging or surgery where patients are either injected in their joint with approximately 10 cc of air and x-ray imaged or given exploratory surgery. A football player injured in a weekend game can be imaged by MRI the same day and given a diagnosis immediately.

Another imaging procedure in which MRI is challenging traditional x-ray procedures is magnetic resonance angiography (MRA) (64, 65). Unlike x-ray-based angiography, MRA does not require the injection of contrast agents into the blood stream. MR angiography images flowing blood as opposed to a contrast agent in a blood vessel. As a consequence MRA can detect locations having poor flow which appear normal on an x-ray angiogram because of the presence of contrast agent in the static blood. Magnetic resonance angiography may be performed by one of two techniques: time-of-flight (64) and phase-contrast (65) angiography. Time-of-flight angiography is performed using a two-step process. First, an image is recorded when the magnetization from

spins flowing into the imaged slice is set to zero by a r-f pulse referred to as a saturating pulse. The second step is to subtract this image from a conventional magnetic resonance image without the saturating pulse. The difference is an image of the flowing blood. Phase-contrast angiography utilizes an extra gradient pulse called a bipolar gradient pulse which imparts a phase shift to the precessional motion of flowing spins. Subtracting an image recorded having a positive bipolar gradient pulse from one recorded having a negative pulse produces an image of flowing blood. Both techniques are routinely used to image flowing blood.

5.3. Safety

Because of the relatively young age of MRI there is concern regarding its safety (66). Users are trying to err on the side of caution. The principal safety concerns are related to the static magnetic field B_0, changing magnetic fields dB_0/dt, tissue heating from r-f power deposition, and acoustic noise. The United States Food and Drug Administration guidelines on static magnetic field limits B_0 to less than 2 T (2×10^4 G). The greatest concern about the health effects of strong magnetic fields are those effects caused by ferromagnetic objects being pulled into the imager while a patient is inside, or the torques created on a ferromagnetic object which might be in the patient's body. A ferromagnetic pen could be pulled into the magnet with sufficient velocity to puncture the body. A ferromagnetic object, such as a metal sliver or an aneurysm clip, located in the patient's body could become reoriented in the field and damage tissues.

The dB/dt is limited to 6 T/s out of concern that larger values could cause nerve stimulation. The r-f exposure is limited to a specific absorption rate (SAR) of 0.4 W/kg for the whole body, 0.32 W/kg averaged over the head, and less than 8.0 W/kg spatial peak in any one gram of tissue. These numbers are designed to limit the temperature rise to less than 1°C and localized temperature of no greater than 38°C head, 39°C trunk, and 40°C in the extremities.

Magnetic resonance imagers produce a loud knocking sound when the magnetic field gradients are turned on or off. The acoustic noise levels can be high in the bore of the magnet. Patients are usually given ear plugs which can decrease the sound of the knocking by upward of 26 dB.

6. Nuclear Medicine Imaging

Nuclear medicine imaging involves the use of exogenous radioactive materials to image the body. The first scientific discovery which made the development of this imaging modality possible was radioactivity by Bacquerel in 1896. Bacquerel shared the Nobel Prize in physics with Pierre and Marja Curie in 1903 for their discoveries related to radioactivity. Another discovery which led to the development of nuclear imaging was that of technetium in 1937. Technetium-labeled molecules, known as radiopharmaceuticals, which have specific biological functions, are used. The first imaging procedures were performed in the 1940s. The presence of a brain tumor was detected and normal and abnormal thyroid functions were investigated. Both experiments used ^{131}I. The Anger scintillation camera, developed in the 1950s, is the primary detector in nuclear medicine. Although the groundwork development of single photon emission computed tomography (SPECT) and positron emission tomography (PET) preceded x-ray-based CT, it was not until the development of CT imaging, and the related reconstruction algorithms, that SPECT and PET were developed to the state of clinical utility.

6.1. Theory and Equipment

The basic principle behind nuclear medical imaging is that a radiopharmaceutical can be introduced into the body which emits radiation detectable outside of the body. Radiopharmaceuticals are biologically active and have a short half-life ($T_{1/2}$). The detectable radiation is typically a γ-ray photon. The radiopharmaceutical must be introduced in sufficient concentration to produce detectable signals outside of the body, but not large enough

Table 4. Radioactive Nuclei Used in Radiopharmaceuticals[a]

Nucleus	Radioactive decay product	γ-Ray energy, keV	$T_{1/2}$	Production[b]
^{201}Tl	γ	70	73 h	CPB
^{133}Xe	γ	81	5.27 d	fission
^{131}I	γ	364	8.05 d	fission
^{123}I	γ	159	13 h	CPB
^{111}In	γ	171, 245	67.9 h	CPB
^{99}Tc^{m}	γ	140.5	6.03 h	^{99}Mo decay
^{82}Rb	β^+	511	1.2 min	^{82}Sr decay
^{67}Ga	γ	93, 184, 300	78.3 h	CPB
^{18}F	β^+	511	110 min	CPB
^{15}O	β^+	511	2 min	CPB
^{13}N	β^+	511	10 min	CPB
^{11}C	β^+	511	20.5 min	CPB

[a]Refs. 21 and 67.
[b]CPB = charged − particle bombardment.

to be lethal. Some radiopharmaceuticals emit γ-rays directly. Other radiopharmaceuticals emit positrons, β^+. Shortly after being emitted, the positron is annihilated when it collides with an electron. Two 511-keV photons are simultaneously produced from the annihilation and possess trajectories 180° apart from each other. The more common radioactive nuclei used in radiopharmaceuticals are listed in Table 4. With the exception of xenon, these nuclei are typically bonded to other atoms or complexed with chelates to form the radiopharmaceutical. The specific structure of the radiopharmaceutical depends on the application.

The radiopharmaceuticals used in nuclear imaging may be produced by either neutron capture, nuclear fission, charged-particle bombardment (CPB) or radioactive decay (21). Neutron capture or activation requires a nuclear reactor, CPB requires an accelerator for production, and radioactive decay production requires a device containing parent nuclei which decay into the desired radiopharmaceutical. Such a device is referred to as a radionuclide generator. Radiopharmaceuticals having a relatively long half-life may be generated off-site or using a radioisotope generated on-site. However, those having shorter half-lives, such as the β^+ emitters, must be generated on-site and thus require a charged-particle accelerator or nuclear reactor.

The radiation emitted by the radiopharmaceutical is most often detected using scintillation detectors of NaI(Tl) (21). The light emitted by a NaI(Tl) scintillator has a wavelength of 410 nm. The intensity of the emitted light is proportional to the energy of the γ-ray photon, therefore a scintillation detector can be used to measure the number of γ-rays and their energy. This violet photon is amplified and converted into an electrical response by a photomultiplier tube. Other γ-ray detectors that have been used in nuclear imaging are multiwire proportional chambers and the lithium-drifted germanium gamma camera.

Gamma radiation may be detected and processed to produce a 2-D planar or a CT emission image. Planar images were first produced using a single detector which moved across the body in a rectilinear motion to produce the planar image of the emitted radiation. Later detectors employed a linear array of 10 or more detectors moved in a linear fashion along the length of the body. More recent designs consist of a flat array of 37 to 91 detectors. The scintillation material is faced with a lead collimator grid, as is done in x-ray imaging. The grid serves as a lens in that it causes the detector to be sensitive to emissions from a specific region of the body. SPECT detectors utilize an array of detectors that move in a manner similar to CT x-ray imaging detectors around the anatomy being imaged.

The scheme used to detect the two 511-keV γ-rays from a β^+ emitter incorporates principles of coincidence detection. The signals from two detectors pointing toward each other along a straight line are processed by circuitry which only produces output when signals are instantaneously detected from each detector. Lead

collimators are placed in front of each detector to minimize scattered and random coincidence. Although planar images could be obtained of the positron emissions from a radiopharmaceutical introduced into the body, positron emission images are typically tomographic. A ring of detectors is arranged around the imaged anatomy. The detectors are connected to an elaborate coincidence logic which registers a signal when any two detectors having a line of sight path between them detects a coincidence. Because a region having a high concentration of β^+ emitter emits many β^+ particles and hence γ-ray coincidences in all directions, a tomographic image may be constructed using the information from all the detectors and the Radon transform. The sensitivity of PET is approximately 20 times greater than that of SPECT because of the coincidence-detection scheme.

6.2. Applications

Brain and central nervous system imaging are common applications of nuclear imaging. Technium-99^m-glucoheptonate [68128-55-2] and $^{99}Tc^m$-DTPA [80908-06-1] are used to study the integrity of the blood brain barrier. Tumors which disrupt the barrier cause these radiopharmaceuticals to pass into the brain. $^{15}O_2$ [95682-06-7] and $C^{15}O_2$ [85401-75-8] can be used to study oxygen uptake by regions of the brain. $H_2{}^{15}O$ [24286-21-3] and ^{133}Xe [14932-42-4] are used to study brain circulation (68). Because the oxygen metabolism and microcirculation in the brain increases during brain activity, these molecules can be used with PET to determine functionality of the various sections of the brain (69). Cerebral blood volume is measured using $^{99}Tc^m$-red blood cells and SPECT.

Cardiac nuclear imaging using $^{99}Tc^m$-red blood cells can measure the fraction of blood pumped by the heart during each beat. $^{99}Tc^m$-DTPA and sodium *o*-iodohippurate, $C_9H^{123}{}_7INNaO_3$, are used to measure renal function of the kidney. The enhanced or diminished uptake of technecium-99^m-methylenediphosphonate [101488-09-9], $^{99}Tc^m(O_3PCH_2PO_3)$, by bones associated with some skeletal abnormalities allows skeletal nuclear imaging. ^{127}Xe [13994-19-9] and $^{81}Kr^m$ [15678-91-8] are used for studies of the respiratory system. $Na^{123}I$ and sodium pertechnetate [13718-28-0], $Na^{99}Tc^mO_4$, are used for imaging of the thyroid gland. Gallium-67-citrate [41183-64-6] is used for tumor imaging. Several other applications of nuclear medicine can be found in the literature (67).

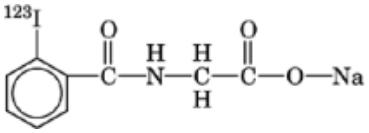

6.3. Safety

The principal concerns regarding nuclear medical imaging are those associated with the radiopharmaceuticals. Much research has gone into the selection of radiopharmaceuticals exhibiting minimal toxicities, rapid elimination from the body, and short half-life. The radioisotope must be nontoxic or capable of being made nontoxic by chelation. These isotopes should have a short half-life so as not to make the body radioactive for a long period of time. Heavy metals, eg, technetium, must be in a form eliminated from the body by the kidneys. The radiopharmaceutical also should not emit harmful amounts of radiation. For example, ^{131}I, a a γ- and β-emitter, in small doses has diagnostic utility in imaging the thyroid. In larger doses, it has therapeutic utility in that it can cause either partial or complete ablation of the thyroid owing to the β-emissions. In addition to health concerns specific to the patient, attention must be paid to minimizing accidental exposure or ingestion of radiopharmaceuticals by the clinical personnel suppressing the imaging procedure.

BIBLIOGRAPHY

Cited Publications

1. D. D. Gibbs, K. F. R. Schiller and P. R. Salmon, eds., *Modern Techniques in Gastrointestinal Endoscopy*, Year Book Medical Publishers, Chicago, 1976, 1–14.
2. A. Kussmaul, *Berichte naturforsch. Ges. Freiburg i. B.* **5**, 112 (1868).
3. M. O. Blackstone, *Endoscopic Interpretation—Normal and Pathologic Appearances of the Gastrointestinal Tract*, Raven Press, New York, 1984.
4. J. F. Rey, M. Albuisson, M. Greff, J. M. Bidart, and J. M. Monget, *Endoscopy* **20**, 8–10 (1988).
5. D. Drez, Jr., *Clin. Sports Med.* **4**, 275–278 (1985).
6. J. W. Segura, *J. Urol.* **132**, 1079–1084 (1984).
7. M. Ohligisser, Y. Sorokin, and M. Hiefetz, *Obstet. Gynecol. Surv.* **40**, 385–396 (1985).
8. R. J. Benzie, *Clin. Obstet. Gynecol.* **7**, 439–460 (1980).
9. P. D. Phillon and J. V. Collins, *Postgrad. Med. J.* **60**, 213–217 (1984).
10. W. Steiner, *Endoscopy* **1**, 51–59 (1979).
11. W. C. Röntgen, *Erste Mitt. Sitzgsber. physik.—med. Ges. Würzburg* **137** (Dec. 1895) transl. A. Stanton, *Nature (Lond.)* **53**, 274–276 (Jan. 23, 1896).
12. E. Hascheck and O. T. Lindenthal, *Wien. klin. Wochenschr.* **9**, 63 (1896).
13. G. N. Hounsfield, *Br. J. Radiol.* **46**, 1016–1022 (1973).
14. H. H. Barrett, W. G. Hawkins, and M. L. G. Joy, *Radiology* **147**, 172 (1983).
15. A. M. Cormack, *J. Appl. Phys.* **34**, 2722–2727 (1963).
16. W. L. Bloom, J. L. Hollenbach, and J. A. Morgan, *Medical Radiographic Technique*, Charles C. Thomas Publishing, Springfield, Ill., 1965.
17. L. F. Squire and R. A. Novelline, *Fundamentals of Radiology*, Harvard University Press, Cambridge, Mass., 1975.
18. T. R. Eastman, *Radiographic Fundamentals and Technique Guide*, C. V. Mosby, St. Louis, Mo., 1979.
19. H. E. Seemann, in J. M. Sturge, ed., *Niblette's Handbook of Photography and Reprography Materials, Processes and Systems*, Van Nostrand Reinhold, New York, 1977, 550–561.
20. L. Erickson and H. R. Splettstosser, in T. H. James, ed., *The Theory of the Photographic Process*, Macmillan, New York, 1977, 662–671.
21. J. T. Bushberg, J. A. Seibert, E. M. Leidholdt Jr., and J. M. Boone, *The Essential Physics of Medical Imaging*, Williams and Wilkins, Baltimore, Md., 1994.
22. Z. H. Cho, J. P. Jones, and M. Singh, *Fundamentals of Medical Imaging*, John Wiley & Sons, Inc., New York, 1993.
23. M. M. Ter-Pogossian, *The Physical Aspects of Diagnostic Radiology*, Harper & Row, New York, 1967.
24. J. L. C. Sanz, E. B. Hinkle, and A. K. Jain, *Radon and Projection Transform-Based Computer Vision*, Springer-Verlag, Berlin, 1988.
25. K. P. Peschmann and co-workers, *Appl. Opt.* **24**, 4052–4060 (1985).
26. J. N. Wolfe, *AJR* **126**, 1130–1137 (1976).
27. J. N. Wolfe, K. A. Buck, M. Salane, and N. J. Parekh, *Radiology* **165**, 305–311 (1987).
28. J. E. Gray, *Proceedings of the Eighteenth Annual Meeting of the National Council on Radiation Protection and Measurements, Radiation Protection and New Medical Diagnostic Approaches*, National Academy of Sciences, Washington, D.C., 1982, 117–129.
29. S. C. Bushong and B. R. Archer, *Diagnostic Ultrasound, Physics, Biology, and Instrumentation.*, Mosby Year Book, St. Louis, Mo., 1991.
30. P. Curie and J. Curie, *Comptes rendus hebdomadaires des séances de l'Académie des sciences* **91**, 294 (1880).
31. *Ibid.*, **93**, 1137 (1881).
32. D. H. Howry and W. R. Bloss, *J. Lab. Clin. Med.* **40**, 579–592 (1952).
33. J. J. Wild and J. M. Reid, *Cancer Res.* **14**, 277–283 (1954).
34. I. Donald, J. MacVicar, and T. G. Brown, *Lancet* **1**, 1188–1194 (1958).

35. R. W. Gill, *Ultrasound Med. Biol.* **11**, 625–641 (1985).
36. J. C. Bamber and M. Tristam, in S. Webb, ed., *The Physics of Medical Imaging*, IOP Publishing, Philadelphia, Pa., 1988.
37. P. N. T. Wells, *Physical Principles of Ultrasonic Diagnosis*, Academic Press, London, 1969.
38. T. Ikeda, *Fundamentals of Piezoelectricity*, Oxford University Press, New York, 1990.
39. K. Kimura, N. Hashimoto, and H. Ohigashi, *IEEE Trans. Sonics Ultrason.* **32**, 566–573 (1985).
40. O. T. vonRamm and S. W. Smith, *IEEE Trans. Biomed. Eng.* **30**, 438–452 (1983).
41. Y. Nomura, Y. Matsuda, I. Yabuuchi, M. Nishioka, and S. Tarui, *Radiology* **187**, 353–356 (1993).
42. R. H. Simon, S. Y. Ho, S. C. Lange, D. F. Uphoff, and J. S. Darrigo, *Ultrasound Med. Biol.* **19**, 123–125 (1993).
43. W. J. Gussenhoven, N. Bom, and J. Roelandt, eds., *Intravascular Ultrasound*, Kluwer, Dordrecht, the Netherlands, 1991.
44. E. A. Neppiras, *Ultrasonics* **24**, 25–28 (1984).
45. F. W. Kremkau, *Clin. Obstet. Gynaecol.* **10**, 395–405 (1983).
46. K. Makino and M. M. Mossoba, *Radiation Res.* **96**, 416–421 (1983).
47. D. D. Stark and W. G. Bradly, *Magnetic Resonance Imaging*, Mosby, Lanham, Md., 1988.
48. C. L. Partain, R. R. Price, J. A. Patton, M. V. Kulkarni, and A. E. James, *Magnetic Resonance Imaging*, Saunders, Philadelphia, Pa., 1988.
49. J. P. Hornak and L. M. Fletcher, in E. R. Dougherty, ed., *Digital Image Processing Methods*, Marcel Dekker, New York, 1994.
50. R. Damadian, *Science* **171**, 1151 (1971).
51. P. G. Lauterbur, *Nature* **242**, 190–191 (1973).
52. A. Kumar, D. Welti, and R. R. Ernst, *J. Magn. Reson.* **18**, 69–83 (1975) *Naturwissenschaften* **62**, 34 (1975).
53. C. P. Slichter, *Principles of Magnetic Resonance*, Springer-Verlag, Berlin, 1980.
54. T. C. Farrar and E. D. Becker, *Pulse and Fourier Transform NMR*, Academic Press, Inc., New York, 1971.
55. E. Fukushima and S. B. W. Roeder, *Experimental Pulse NMR*, Addison-Wesley, Reading, Mass., 1981.
56. R. C. Weast, ed., *CRC Handbook of Chemistry and Physics*, 53rd ed., CRC Press, Cleveland, Ohio, 1972.
57. S. L. Smith, *Anal. Chem.* **57**, A595–A607 (1985).
58. C. E. Hayes, W. A. Edelstein, and J. F. Schenck, in C. L. Partain, R. R. Price, J. A. Patton, M. V. Kulkarni, and A. E. James, eds., *Magnetic Resonance Imaging*, Saunders, Philadelphia, Pa., 1988.
59. G. M. Bydder, in D. D. Stark and W. G. Bradley, eds., *Magnetic Resonance Imaging*, Mosby, Lanham, Md., 1988.
60. J. H. Bisese, *Cranial MRI: A Teaching File Approach*, McGraw-Hill Book Co., Inc., New York, 1991.
61. S. Ogwa and co-workers, *Proc. Mat. Acad. Sci.* **89**, 5951–5955 (1992).
62. P. Mansfield, *J. Phys. C: Solid State Phys.* **10**, L55 (1977).
63. M. Dunitz, *MRI Atlas of the Musculoskeletal System*, CRC Press, Boca Raton, Fla., 1989.
64. D. G. Nishimura, *Magn. Reson. Med.* **14**, 194–201 (1990).
65. C. L. Dumoulin, S. P. Souza, M. F. Walker, and W. Wagle, *Magn. Reson. Med.* **9**, 139–149 (1989).
66. J. Leigh, *Resonance Newsletter SMRM*, **20**, 9 (1990).
67. R. J. Ott, M. A. Flower, J. W. Babich, and P. K. Marsden, in Ref. 36.
68. M. E. Raichle, *Sci. Am.* **270**, 58–64 (1994).
69. K. F. Hubner, J. Collmann, E. Buonocore, and G. W. Kabalka, *Clinical Positron Emission Tomography*, Mosby Year Book, St. Louis, Mo., 1991.

JOSEPH P. HORNAK
Rochester Institute of Technology

Related Articles

Nondestructive evaluation; Photodetectors; Magnetic spin resonance